crystals

MDPI

Article

Surface Plasmon Resonance and Increased Interfacial Electron Transfer of 3D AgNWS@TiO_2NS Structure for Enhanced Photocatalytic and DSSC Properties

Fengyang Zhao [1] and Yongjian Jiang [2,*]

[1] College of Chemistry and Material Science, Liaoning Petrochemical University, Fushun 113001, China; zhaofengyang@lnpu.edu.cn
[2] College of Science, Liaoning Petrochemical University, Fushun 113001, China
* Correspondence: jiangyongjian@lnpu.edu.cn; Tel.: +86-024-56861865

Abstract: Ag nanowires coated with TiO_2 nanosheets (AgNWS@TiO_2NS, AWT) have been successfully synthesized via a one-pot hydrothermal synthesis. Importantly, the prepared AWT shows enhanced photocatalytic activity compared with Degussa P25, which is attributed to its continuous hierarchical structures, special conductive channel and localized surface plasmon resonance (SPR). Additionally, these prepared AWT were exploited as an electron conductor and scattering material in the TiO_2 composite photoanodes of dye-sensitized solar cells (DSSCs). The highest energy conversion efficiency of 6.98% was achieved when the AWT doping rate in the photoanode slurry was 5 wt%. Both enhanced Isc and Voc are attributed to the increased photo-absorption efficiency from the localized SPR. The potential enhanced light-scattering effect and faster photoelectric transmission efficiency of the AWT in the photoanode.

Keywords: AgNWS@TiO_2NS; photocatalytic; scattering layer; DSSCs; surface plasmonic response

check for updates

Citation: Zhao, F.; Jiang, Y. Surface Plasmon Resonance and Increased Interfacial Electron Transfer of 3D AgNWS@TiO_2NS Structure for Enhanced Photocatalytic and DSSC Properties. *Crystals* **2022**, *12*, 498. https://doi.org/10.3390/cryst12040498

Academic Editors: Masakazu Anpo and Stefano Carli

Received: 26 February 2022
Accepted: 2 April 2022
Published: 3 April 2022

Publisher's Note: MDPI stays neutral with regard to jurisdictional claims in published maps and institutional affiliations.

Copyright: © 2022 by the authors. Licensee MDPI, Basel, Switzerland. This article is an open access article distributed under the terms and conditions of the Creative Commons Attribution (CC BY) license (https://creativecommons.org/licenses/by/4.0/).

1. Introduction

Solar energy is one kind of energy that is renewable and clean. In recent years, it has become the hottest issue of studies to utilize local abundant solar energy resource to replace prevenient energy consumption. A large number of studies confirmed that TiO_2 have many advantages, such as their excellent photocatalytic performance, and high photoelectric conversion, low-power and low-cost, easy manufacture, and potential business prospects [1–3]. As we know, TiO_2 is a wide bandgap semiconductor material, and its bandgap is 3.2 ev for anatase TiO_2 [4]. So conventional titanium dioxide absorbs only the ultraviolet part of sunlight, which makes up about 5 percent of the sun's rays. In past years, a large number of studies have shown that the absorption spectrum range of TiO_2 in sunlight can be expanded by means of ion doping, precious metal composite and sensitizer sensitization [5–7].

In 1972, Dye-Sensitized Solar Cells (DSSC) were invented successfully [8]. The core of the DSSC system is the photo-anode film composed by the nanometer to micron mesoporous structure [9–11]. However, the classical mesoporous photo-anode only contains TiO_2 nanoparticles [12]. The slow electron transport, considerably high carrier recombination losses, and inefficient light harvesting are deemed as the three key factors that limit the development of high-performance DSSCs with only TiO_2 nanoparticle photoanodes [13–15]. People have shown great interest in plasmonic solar cells [16–19]. The surface plasmon arising from 1D Ag nanowires (AgNWs) has been applied to increase light-harvesting and electron transferring and reduce the carrier recombination. However, when Ag nanowires are in direct contract with the electrolyte or the dye in DSSCs, cell efficiency decreases because AgNWs acts as a recombination center for photo generation [20,21]. A practical method to surmount these shortcomings is to initiate a novel core-shell structure consisting

of Ag core and TiO_2 nanostructure sheets [22]. The electrons formed by illumination can be transferred from TiO_2 nanoshell to silver nanowires as soon as possible in the Ag/TiO_2 core-shell heterostructure (AgNWS@TiO_2NS). In other words, AgNWS@TiO_2NS increases the electron transport, thus reducing the e-/h+ recombination probability [23].

Meanwhile, materials with scattering property can increase the photoelectron propagation pathways against the low wave region of the solar spectrum in the photoanodes by surface plasmon response (SPR) effects [24,25]. One essential issue that needs to be addressed when considering possible applications of AgNW@TiO_2NS in DSSCs is that the small area of AgNW@TiO_2NS should be destined to decrease the dye adsorption thus leading to low light efficiency. Therefore, the preparation of composite photoanodes, including AgNWS@TiO_2NS and TiO_2 nanoparticle films, is urgently needed. In recent years, more and more research has been focused on SPR, and have made it being applied successfully in many areas [24].

In our work, AgNWS@TiO_2NS (AWT) was prepared via a simple hydrothermal synthesis. It is worthy to note that the prepared 3D AgNWS@TiO_2NS superstructures exhibit higher photocatalytic activity than Degussa P25 for the degradation of methyl orange (MO) under UV light irradiation. Then, AWT was employed in the photoanodes of the DSSCs by incorporating AWT in TiO_2 P25 nanoparticles with different mass ratios (0%, 0.5%, 1%, 5%, 10%, and 20%). The highest photoelectric transformation efficiency of 6.98% is achieved for DSSC with 5% AWT in the photoanode. This improvement could result from multiple factors, including the decreased electron transfer resistance in TiO_2/dye/electrolyte boundary, the enhanced surface plasmon resonance of AgNWs, and the light scattering effects of the 3D structures in the photoanode of DSSCs.

2. Materials and Methods

The AWT was synthesized by a one-step hydrothermal synthesis method. Tetrabutyl titanate (TBOT) was used as the precursor for the growth of nanostructures on the surface of Ag nanowires. Experimental procedures were as follows: 20 mg of silver nanowire powder was weighed to be dispersed in 10 mL of ethanol solution with magnetic stirring for 30 min. Then 15 ul of TBOT was measured by slowly dropping into the above-mixed dispersion followed by stirring for 30 min before the solution became homogeneous. The reaction was conducted in a 50 mL autoclave with a treatment at 200 °C for 12 h. After the hydrothermal reaction process, the samples were washed with deionized water, separated by centrifugation, and dried naturally. Finally, it was calcined in a Muffle furnace at 450 °C for 1 h. Formulation and sizing technique: 3 g P25 and AWT powder, 0.1 mL acetic acid, 7.9 mL deionized water, and 0.2 mL Triton X-100 were first prepared as comparison material. Then, the different mass ratios (AgNWs contents: 0.5 wt%, 1 wt%, 5 wt%, 10 wt%, and 20 wt%) of AWT were incorporated into the slurry as mentioned above. In our previous work, we have presented the scraping, sensitized photoanode films, and encapsulation of DSSCs in detail [3]. Pt electrodes were purchased from Dalian Qi Se guang Optical Technology Development. The thickness is 2 μm, the effective area is 8*8 mm, and the aperture is 1 mm. The thickness of the composite photoanodes is approximately 13 μm. N719 dye ($C_{58}H_{86}N_8O_8RuS_2$) and Liquid electrolyte (DHS-E23; solvent:acetonitrile; redox couple: I^{3-}/I^-) (Dalian Heptachroma Solar Tech, Co., Ltd.). All materials were used as received [3].

The morphology of the AWT was observed by scanning electron microscopy (SEM, FEI SIRION 200) and high-resolution transmission electron microscopy (TEM/HRTEM, JEM-200CX) equipped with selected area electron diffraction (SAED) of the samples. X-ray powder diffraction (XRD) was performed on the prepared AWT for phase analysis. The photocatalytic degradation of methyl orange was described in detail in our previous work. The diffuse reflectance spectra of photoanodes were measured using a UV-Vis spectrophotometer (UV 2600 Shimadzu). The various photoanodes' dye loading capacity was subsequently determined using the same methodology described in our previous work [2]. These cells' photovoltaic performance, electrochemical impedance spectra (EIS),

and incident-photon-current efficiency (IPCE) were also determined as described in previous work [2].

3. Results and Discussion

The TEM outcomes of Ag nanowires are shown in Figure 1a. We can see that these Ag nanowires featured a smooth surface with a high aspect ratio whose diameter was about 80 nm. In contrast, the SEM and TEM of the AWT had a rough surface with uniform small TiO_2 nanosheet coatings wrapped on the surface of the Ag nanowires (Figure 1b,c). Unusually, the new structure presents a very uniform appearance.

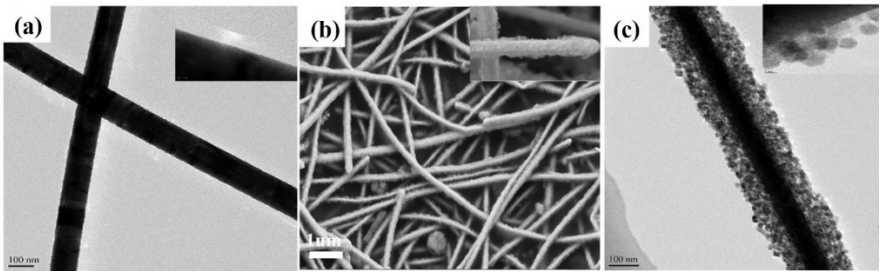

Figure 1. TEM images of Ag nanowires (**a**) (insert: high magnification); SEM of AWT after 450 °C calcinated (**b**) (insert: SEM image); TEM of AWT after 450 °C calcinated (**c**) (insert: HRTEM image).

Figure 2a shows the SEM photograph of the AWT, further confirming that the prepared Ag@TiO_2 has a homogeneous core-shell structure. It can be seen that the TiO_2 nanosheet layer is uniformly covered the surface of Ag nanowires, leading the diameter of AWT to increase to 200 nm approximately. These tightly bonded core/shell structures might support that it is favorable to separate electrons and holes and preferential photoelectron transport from the TiO_2 shell to the Ag cores [26]. In the meantime, the composition structure determined by Energy Dispersive Spectrum (EDS) is a better analysis of the crystal structures. Figure 2b shows the element spectrum at the position of the marked information in Figure 2a. We can observe the presence of silver, Ti, and O elements in the sample. Meanwhile, the XRD pattern of Ag@ TiO_2 was further detected. As shown in Figure 2c, three different diffraction peaks corresponding to the (111), (220), and (311) planes of the Ag crystal were observed for the obtained AWT sample. Moreover, the prominent diffraction peaks of (101) at 25.37° and (200) at 48.12° can also be tested in Figure 2c. It demonstrated the existence of anatase TiO_2. On the basis of the experimental data, we deduced that the framework of the Ag nanowires has remained unchanged during the hydrothermal process. Therefore, it can be inferred that the structures formed during the hydrothermal reaction are only anatase-type TiO_2 nanosheets.

The HRTEM image also clearly reveals the core-shell structure (Figure 2d). It can be seen that the TiO_2 shells consist of interconnected nanosheets. The corresponding high-resolution photos are shown in Figure 2e,f. The fringe spacings of 0.236 nm and 0.35 nm correspond well to the lattice space of (001) and (101) of anatase TiO_2 [26,27]. It is compatible with the XRD data. Meanwhile, the corresponding electron diffraction patterns (EDP) indicated that the TiO_2 nanosheets were polycrystalline structures (Figure 2g). However, we also found that there was a certain amount of amorphous TiO_2 structure in the generated nanosheets, as shown in the Figure 2d.

The photocatalytic degradation of methyl orange (MO) by Ag/TiO_2 heterostructure was carried out at room temperature, and the same experiment was performed on commercial P25. The specific reaction process has been described below: 0.02 g P25, AWT photocatalyst powder was dispersed in 20 mL MO solution with a concentration of 2 mg/L by ultrasound and stirred under dark conditions for 1 h to achieve adsorption balance between the degradation material and the catalyst.

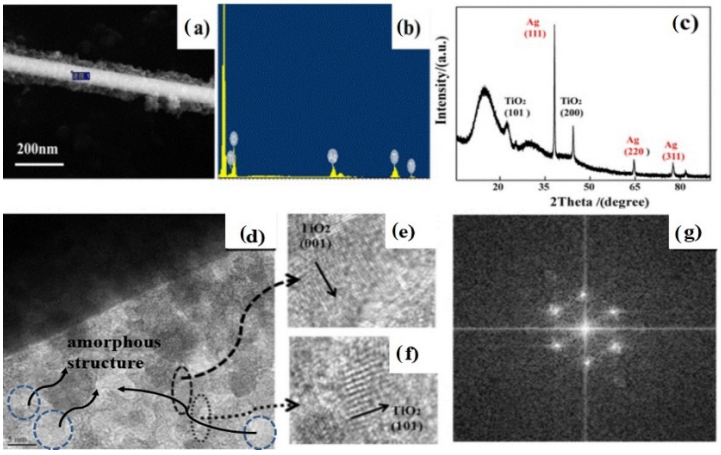

Figure 2. SEM image (**a**); EDS (**b**); XRD pattern (**c**) of a single root AWT obtained from a 12-h hydrothermal reaction; TEM (**d**) of the AWT obtained after a 1-h calcined process; the corresponding lattice fringes (**e**) and (**f**); the corresponding electron diffraction patterns (EDP) (**g**).

P25 and AWT adsorption experiment was carried out by ultraviolet-visible spectrophotometer first, after the methyl orange solution to reach adsorption equilibrium, MO remaining in the solution within the scope of the ultraviolet-visible absorption spectra as shown in Figure 3a, the MO solution on AWT as photocatalyst in 60 min after the adsorption equilibrium of presents the weakest light absorption, which suggests that AWT adsorbed more methyl orange molecules under dark conditions, most likely due to the effect of two-dimensional TiO_2 nanosheet, because of its excellent two-dimensional nanosheets, AWT adsorbed more methyl orange molecules under dark conditions, while commercial P25 had weaker adsorption capacity, which also indicated that AWT had certain advantages in organic pollutant adsorption and N719 dye adsorption in the follow-up work.

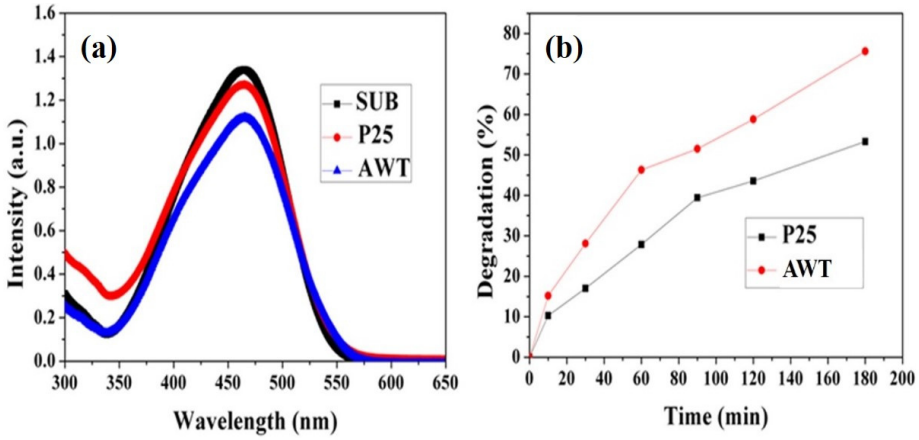

Figure 3. (**a**) UV-Vis adsorption spectra of the P25 and AWT after being stirred in the dark in MO solution for 60 min at room temperature; (**b**) photocatalytic degradation of MO by different photocatalysts under UV light irradiation.

Then, in order to systematically analyze the degradation rate of methyl orange by photocatalyst, the stirred solution was taken for 10 min, 30 min, 60 min, 90 min, 120 min and 180 min during the UV light reaction, respectively. Degradation rate curves of AWT and P25 can be obtained by using degradation rates of MO at different times as ordinate. As shown in Figure 3b, AWT showed a faster degradation rate than commercial P25. After 180 min, the degradation rate of MO solution using AWT as photocatalyst reached 75 %, while that of P25 was 53 %. AWT showed excellent degradation performance mainly due to the following points. First, Ag nanowire is not only the growth scaffold of TiO_2 two-dimensional nanosheet layer, but also provides a fast electron transport channel, which will

greatly reduce the recombination rate of the electron hole [28]. Second, in addition to the heterostructure of Ag nanowire and TiO_2 two-dimensional nanosheet surface, the Schottky barrier formed between Ag nanowire and TiO_2 semiconductor also plays an important role in the improvement of photocatalysis. Schottky barrier can be used as an electron trap to facilitate photoinduced electron and hole separation, thus improving the catalytic activity of AWT [28].

We assembled DSSCs consisting of TiO_2 P25 photoanodes doped with different AWT. The properties were investigated by testing and analyzing the optoelectronic characteristics. As a comparison, the pure TiO_2 P25 photoanode DSSC was also investigated. The current-voltage (IV) curves for the composite photoanodes (AWT/P25- DSSCs) are shown in Figure 4. As shown in Table 1, the AWT-5 DSSC showed the best photoelectric performance among these composites, achieving a conversation efficiency of 6.98 %.

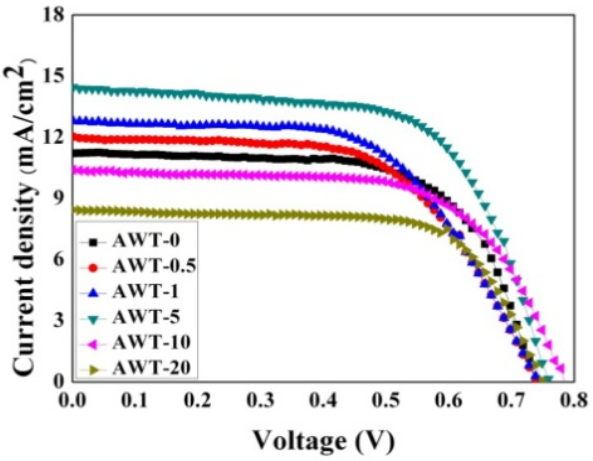

Figure 4. I-V curves of cells based on AWT-0, AWT-0.5, AWT-1, AWT-5, AWT-10, and AWT-20 composite films electrodes.

Table 1. Performance parameter characteristics of DSSCs based on different AWT/P25 photoanode films.

Samples	AWT (wt%)	J_{SC} (mA/cm^2)	Voc (V)	FF	PCE (%)	Rct (Ω)
AWT-0	0	11.23	0.74	0.652	5.42	24
AWT-0.5	0.5	12.03	0.75	0.608	5.48	22
AWT-1	1	12.80	0.75	0.578	5.55	20
AWT-5	5	14.46	0.76	0.635	6.98	19
AWT-10	10	10.40	0.79	0.633	5.20	20
AWT-20	20	8.44	0.76	0.681	4.31	35

In addition, the short-circuit current density (Jsc) significantly changed as the AWT in the photoanode film increased. By systematic analysis, the Jsc increased in a monotonic manner when the AWT content was increased from 0 % to 5 wt%. However, when the AWT was further increased, Jsc decreased. The optimum Jsc value of 14.46 mA cm^{-2} was achieved in the device with 5 % AWT, which is significantly better than without AWT (11.23 mA cm^{-2}). The increase in Jsc would be associated with the enhanced light scattering caused by SPR in the visible range. It would reduce the transmission of incident light and increase the effective optical path, allowing the dye molecules to capture photons and convert them into charge carriers.

Nevertheless, the Jsc in DSSCs was reduced when the AWT exceeded 5 wt%. With the increase in the AWT doping ratio, amorphous TiO_2 increased significantly, which will reduce electron mobility and thus reduce the photocurrent generation of the composite photoanode DSSC. As a result, it reduces the photoelectric conversion efficiency of the cell.

To better understand the photovoltaic behavior of different photoanode-based DSSCs, the incident photon pair current efficiency (IPCE) spectrum was measured. IPCE is one

of the essential performance parameters for DSSCs [29]. Figure 5a shows the IPCE curves for different DSSCs. It can be observed that in the wavelength range of 400–700 nm, the IPCE of DSSCs with AWT (0.5–5 wt%) is significantly enhanced. Firstly, the SPR of Ag nanowires can capture the incident light in a specific range and increase the light collection performance in the whole wavelength range. Secondly, the Ag nanowires are relatively large in structure, scattering the incident light and increasing the optical path for composite photoanodes DSSCs. It is observed that the light scattering effect contributes to the enhancement of IPCE in the long light wave region. Nevertheless, when the containing AWT exceeds 5 wt%, the IPCE curves decline drastically. This result can be explained as follows: excessive AWT can reduce the yield of photogenerated electrons of the photoanode film, thereby reducing the IPCE efficiency.

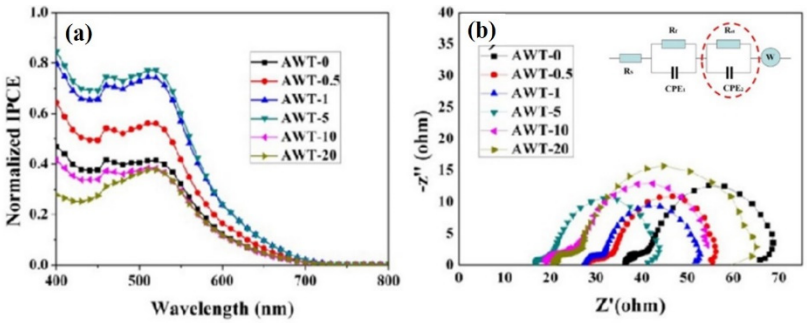

Figure 5. (**a**) Normalized IPCE and (**b**) Nyquist plots for DSSCs: AWT-0, AWT-0.5, AWT-1, AWT-5, AWT-10, and AWT-20 composite films electrodes; the inset image of (**b**) is the equivalent circuit.

Electrochemical impedance spectroscopy (EIS) serves as a robust measurement approach to study charge transfer, charge recombination, and electron transport towards the photoanode interface [30]. EIS Nyquist plots were obtained by measuring the DSSCs. As shown in Figure 5b, the corresponding equivalent circuit diagram is shown inside it, the results of each test in the plot were shown for two semicircles. We called them Z1 and Z2, which represent the impedance spectra of charge transfer at the Pt/electrolyte interface and the impedance spectra of the TiO_2/dye/electrolyte interface, respectively. The inset image of Figure 5b represents the corresponding equivalent circuit diagram for a DSSC. CPE is the constant phase element, and W is the Warburg element and accounts for diffusion of the electrolyte [31]. Where no other impedances elements change, we were only focused on the electron transfer at the photoanode/dye/electrolyte interface, corresponding to the charge transfer resistance Rct (the right part of Z2). The diameter of Z2 reduced in a monotonous manner as the AWT content of the photoanode film increased from 0–5 wt% (Figure 5b). At the same time, the corresponding charge transfer resistance was obtained by the analog circuit fitting process. The charge transfer resistance Rct decreased from 24 Ω of P25-DSSC to 19 Ω of P25/AWT-DSSC, and the optimal AWT content was 5 wt%. It means that if the diameter of Z2 in the Nyquist diagram has been smaller, then the amount of electron recombination reaction at the TiO_2/dye/electrolyte interface would be minimized with a greater J_{SC}. Nevertheless, the diameter of Z2 increased with increasing AWT. It may be due to the excess amorphous structures in AWT leading to accelerate the recombination of electron-hole pairs in TiO_2.

The reflection effect of AWT on the light absorption of photoanode dye was also studied. The reflectance spectra of different photoanode films after absorbing dyes were measured. It can be observed from the Figure 6a, the reflectance curve of AWT-doped photoanode films is significantly different from that of simple P25 photoanode film, which also indicates that the light reflection effect of composite photoanode film tends to increase in visible light. This also demonstrates the strong light scattering ability of AWT continuous three-dimensional structure. As a confirmation of the reasoning, the dye-adsorption capacity of the various photoanode films was also tested. The absorption spectra of desorption experiments by NaOH treated are shown in Figure 6b.

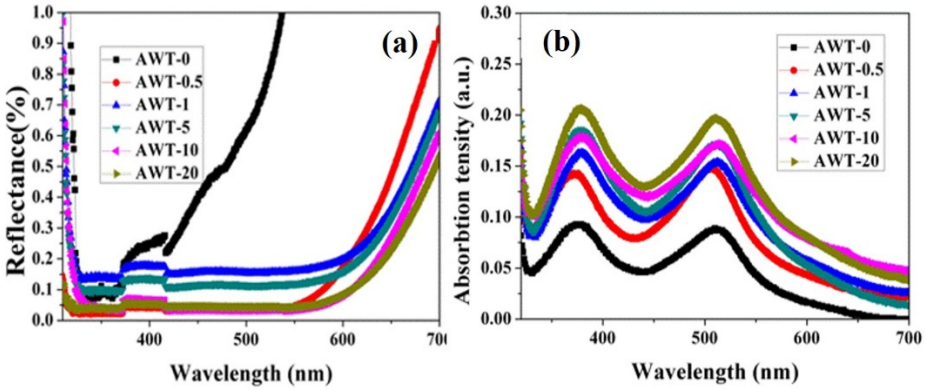

Figure 6. (**a**) Reflectance spectra for the composite electrode films after N719 desorption attached and (**b**) absorption spectra for the composite electrode films after the dye uptaking process.

It is noteworthy that the absorption peaks of AWT-containing photoanode film desensitized solution are significantly enhanced at 375 nm and 512 nm compared with pure P25 film. The results show that the special two-dimensional structure increases the dye adsorption capacity, and the dye load of TiO_2 photoanode film containing AWT is higher than that of pure P25 photoanode film. It can be seen from the above results that the enhancement of light absorption capacity of 0–5 wt% composite photoanode film is not only due to the increase of dye absorption capacity. It is also benefited from the scattering effect of SPR and AWT that made the sunlight utilization rate of photoanode film is significantly improved.

4. Conclusions

In summary, we have successfully synthesized a novel 3D composite nanostructure that consists of a TiO_2 nanosheet shell and an Ag nanowire core (AWT). The novel TiO_2 material exhibits better photocatalytic performance for the degradation of MO compared with Degussa P25, which is attributed to its continuous hierarchical structures, special conductive channel and localized SPR effect. Then a series of AWT/TiO_2 composite photoanode films were prepared and applied to DSSCs. The experimental result indicated that the light absorption range, light absorption ability, and light scattering ability of dye molecules improved when AWT was added to the composite photoanode. The cell exhibited the highest photoelectric conversion efficiency (J_{SC} of 14.46 mA cm^{-2} and η of 6.98 %) with an AWT content of 5 wt%, which was superior to that of P25-DSSC. The enhancement of J_{SC} and η was attributed to the effective optical coupling, light scattering, and dye absorption by the SPR of AWT in the photoanode. Simultaneously, the increase in V_{OC} in the DSSC of AWT may be attributed to the direct electrical transport pathway of photogenerated electrons provided by the Ag nanowires.

Author Contributions: Formal analysis, F.Z.; Funding acquisition, F.Z. and Y.J.; Investigation, Y.J.; Software, Y.J.; Writing—original draft, Y.J.; Writing—review and editing, F.Z.. All authors have read and agreed to the published version of the manuscript.

Funding: The work was supported by National Natural Science Foundation of China (No. 21808096); Fundamental Research Funds for the Doctors of Liaoning Provincial Natural Science Foundation (No. 20170520259); Scientific Research Fund of Liaoning Provincial Education Department (NO. L2017LQN003, L2017LQN036) and Talent Scientific Research Fund of LSHU (No. 2016XJJ-071, 2016XJJ-088).

Data Availability Statement: The study did not report any data.

Conflicts of Interest: The authors declare no conflict of interest.

References

1. O'regan, B.; Gratzel, M. A Low Cost and High Efficiency Solar Cell Based on Dye Sensitized Colloidal TiO_2 films. *Nature* **1991**, *353*, 737–740. [CrossRef]
2. Jiang, Y.J.; Li, M.C.; Ding, R.Q.; Song, D.D.; Mwenya, T.; Chen, Z. Enhanced the performance of dye-sensitized solar cells with a novel photoanode using TiO_2 nanoflflower clusters and nanoparticles. *Mater. Lett.* **2013**, *107*, 210–213. [CrossRef]
3. Zhao, F.Y.; Ma, R.; Jiang, Y.J. Strong effificiency improvement in dye-sensitized solar cells by novel multi-dimensional TiO_2 photo electrode. *Appl. Surf. Sci.* **2018**, *434*, 11–15. [CrossRef]
4. Nakatani, H.; Hamachi, R.; Fukui, K.; Motokucho, S. Synthesis and activity characteristics of visible light responsive polymer-photocatalyst system with a styrene block copolymer containing TiO_2 gel. *J. Colloid Interface* **2018**, *532*, 210–217. [CrossRef] [PubMed]
5. Zhang, S.B.; Zhao, Y.C.; Yang, J.P.; Zhang, J.Y.; Zheng, C.G. Fe-modified MnOx /TiO_2 as the SCR catalyst for simultaneous removal of NO and mercury from coal combustion flue gas. *Chem. Eng. J.* **2018**, *348*, 618–629. [CrossRef]
6. Ton, N.N.T.; Dao, A.T.N.; Kato, K.; Ikenaga, T.; Trinh, D.X.; Taniike, T. One-pot synthesis of TiO_2 / graphene nanocomposites for excellent visible light photocatalysis based on chemical exfoliation method. *Carbon* **2018**, *133*, 109–117. [CrossRef]
7. Ji, L.J.; Zhang, Y.H.; Miao, S.Y.; Gong, M.D.; Liu, X. Insitu synthesis of carbon doped TiO_2 nanotubes with an enhancedphoto catalytic performance under UV and visible light. *Carbon* **2017**, *125*, 544–550. [CrossRef]
8. Fujishima, A.; Honda, K. Electrochemical photolysis of water at a semiconductor electrode. *Nature* **1972**, *238*, 37–38. [CrossRef]
9. Kong, F.T.; Dai, S.Y.; Wang, K.J. Review of recent progress in dye-sensitized solar cells. *Adv. Optoelectron.* **2007**, *2007*, 75384. [CrossRef]
10. Jose, R.; Thavasi, V.; Ramakrishna, S. Metal oxides for dye-sensitized solar cells. *J. Am. Ceram. Soc.* **2009**, *92*, 289–301. [CrossRef]
11. Hagfeldt, A.; Boschloo, G.; Sun, L.; Kloo, L.; Pettersson, H. Dye-sensitized solar cells. *Chem. Rev.* **2010**, *110*, 6595–6663. [CrossRef] [PubMed]
12. Jang, H.D.; Jo, E.H.; Chang, H. Incorporation of 3D crumpled graphene in nanostructured TiO_2 films for dye-sensitized solar cells. *Mater. Lett.* **2015**, *142*, 304–307. [CrossRef]
13. Zhao, Y.L.; Song, D.M.; Qiang, Y.H. Dye-sensitized solar cells based on TiO_2 hollow spheres/TiO_2 nanotube array composite films. *Appl. Surf. Sci.* **2014**, *309*, 85–89. [CrossRef]
14. Wang, G.X.; Zhu, X.J.; Yu, J.G. Bilayer hollow/spindle-like anatase TiO_2 photoanode for high efficiency dye-sensitized solar cells. *J. Power Sources* **2015**, *278*, 344–351. [CrossRef]
15. Nazeeruddin, M.K.; Splivallo, R.; Liska, P. A Swift Dye Uptake Procedure for Dye Sensitized Solar Cells. *Chem. Commun.* **2003**, *12*, 1456–1457. [CrossRef] [PubMed]
16. Shivaprasad, M.; Vasavidutt, V.G.; Phanikumar, K.K.; Atchuta, S.R.; Anbazhagan, V.; Sakthivel, S. A functional Ag-TiO_2 nanocomposite solar selective absorber with antimicrobial activity by photochemical reduction process. *J. Photochem. Photobiol. B* **2019**, *19*, 111626.
17. Wu, W.Y.; Hu, C.F.; Wu, M.J.; Chen, C.N.; Huang, J.J. Ag–TiO_2 composite photoelectrode for dye-sensitized solar cell. *Appl. Phys. A Mater. Sci. Process.* **2017**, *123*, 357. [CrossRef]
18. Wei, X.; Nbelayim, P.S.; Kawamura, G.; Muto, H.; Matsuda, A. Ag nanoparticle-filled TiO_2 nanotube arrays prepared by anodization and electrophoretic deposition for dye-sensitized solar cells. *Nanotechnology* **2017**, *28*, 13. [CrossRef]
19. Eli, D.; Ahmad, M.S.; Bikimi, A.B.; Babatund, O.A. Plasmonic Dye Sensitized Solar Cells Incorporated with TiO_2-Ag Nanostructures. *Int. Res. J. Pure Appl. Chem.* **2016**, *11*, 1–7. [CrossRef]
20. Wang, L.Q.; Jia, L.S.; Li, Q.B. A novel sulfur source for biosynthesis of (Ag, S)-modified TiO_2 photoanodes in DSSC. *Mater. Lett.* **2014**, *123*, 83–86. [CrossRef]
21. Qi, J.; Dang, X.; Hammond, P.T.; Belcher, A.M. High efficient plasmon-enhanced dye-sensitized solar cells through metal@oxidecore-shellnanostructure. *ACS Nano* **2011**, *5*, 7108–7116. [CrossRef] [PubMed]
22. Fallah, M.; Maleki, I.; Meymian, M.R.Z.; Abdi, Y. Enhancing the efficiency of dye-sensitized solar cell by increasing the light trapping and decreasing the electron-hole recombination rate due to Ag@TiO_2 core-shell photoanode structure. *Mater. Res. Express* **2020**, *7*, 016409. [CrossRef]
23. Honda, M.; Kumamoto, Y.; Taguchi, A.; Saito, Y.; Kawata, S. Plasmon-enhanced UV photocatalysis. *Appl. Phys. Lett.* **2014**, *104*, 61108. [CrossRef]
24. Pang, C.; Li, R.; Zhang, Y.; Li, Z.; Dong, N.; Wu, L.; Yu, H.; Wang, J.; Ren, F.; Chen, F. Tailoring optical nonlinearities of $LiNbO_3$ crystals by plasmonic silver nanoparticles for broadband saturable absorbers. *Opt. Express.* **2018**, *26*, 31276–31289. [CrossRef] [PubMed]
25. Li, R.; Dong, N.; Ren, F.; Amekura, H.; Wang, J.; Chen, F. Nonlinear absorption response correlated to embedded Ag nanoparticles in BGO single crystal: From two-photon to three-photon absorption. *Sci. Rep.* **2018**, *8*, 1977. [CrossRef] [PubMed]
26. Pang, C.; Li, R.; Huang, J.W.; Li, Z.Q.; Chen, M.; Dong, N.N.; Wang, J.; Ren, F.; Chen, F. Ultrafast electron transfer dynamics in Ag/TiO_2 nanocomposite for tailoring of optical nonlinearity. *Appl. Surf. Sci.* **2021**, *539*, 148258. [CrossRef]
27. Zhen, M.M.; Jiang, K.L.; Guo, S.Q.; Shen, B.X.; Liu, H.L. Suitable lithium polysulfides diffusion and adsorption on CNTs@TiO_2-bronze nanosheets surface for high-performance lithium-sulfur batteries. *Nano Res.* **2022**, *15*, 933–941. [CrossRef]
28. Wang, Y.; Zhai, J.; Song, Y.L. Feather-like Ag@TiO_2 nanostructures as plasmonic antenna to enhance optoelectronic performance. *Phys. Chem. Chem. Phys.* **2015**, *17*, 5051. [CrossRef]

29. Fisher, A.C.; Peter, L.M.; Ponomarev, E.A.; Walker, A.B.; Wijayantha, K.G.U. Intensity dependence of the back reaction and transport of electrons in dye-sensitized nanocrystalline TiO_2 solar cells. *J. Phys. Chem. B* **2000**, *104*, 949–958. [CrossRef]
30. Wang, Q.; Moser, J.E.; Gratzel, M. Electrochemical Impedance Spectroscopic Analysis of Dye-Sensitized Solar Cells. *J. Phy. Chem. B* **2005**, *109*, 14945–14953. [CrossRef]
31. Park, J.T.; Chi, W.S.; Roh, D.K.; Ahn, S.H.; Kim, J.H. Hybrid Templated Synthesis of Crack-Free, Organized Mesoporous TiO_2 Electrodes for High Efficiency Solid-State Dye-Sensitized Solar Cells. *Adv. Funct. Mater.* **2013**, *23*, 26–33. [CrossRef]